



Imaging Biomarkers in Oncology: Basics and Application to MRI

Isabel Dregely, PhD ¹, Davide Prezzi, FRCR,^{2,3} Christian Kelly-Morland, FRCR,^{2,3}
Elisa Roccia, MRes,¹ Radhouene Neji, PhD,^{1,4} and Vicky Goh, FRCR ^{2,3*}



CME Information: Imaging Biomarkers in Oncology: Basics and Application to Magnetic Resonance Imaging (MRI)

If you wish to receive credit for this activity, please refer to the website: www.wileyhealthlearning.com

Educational Objectives

Upon completion of this educational activity, participants will be better able to:

- Name and describe established and emerging magnetic resonance imaging biomarkers for diagnosis, prognosis and response assessment in cancer imaging
- Describe the key principles for imaging biomarker development

Activity Disclosures

No commercial support has been accepted related to the development or publication of this activity.

Faculty Disclosures:

Editor-in-Chief: Mark E. Schweitzer, MD, discloses consultant fees from MCRA and MMI.

CME Editor: Mustafa R. Bashir, MD, discloses research support from GE Healthcare, Madrigal Pharmaceuticals, NGM Biopharmaceuticals, Siemens Healthcare and Taiwan J Pharma, and consultant fees from RadMD.

CME Committee:

Bonnie Joe, MD, PhD, discloses author royalties from UpToDate.

Tim Leiner, MD, PhD, discloses research grants from Bayer Healthcare and Philips Healthcare.

Shreyas Vasanawala, MD, PhD, discloses research support from GE Healthcare, and founder's equity in Arterys.

Eric Chang, MD, Feng Feng, MD, and Bruno Madore, PhD; no conflicts of interest or financial relationships relevant to this article were reported.

Authors:

Isabel Dregely, Davide Prezzi, Christian Kelly-Morland, Elisa Roccia, Radhouene Neji, and Vicky Goh; no conflicts of interest or financial relationships relevant to this article were reported.

This activity underwent peer review in line with the standards of editorial integrity and publication ethics. Conflicts of interest have been identified and resolved in accordance with John Wiley and Sons, Inc.'s Policy on Activity Disclosure and Conflict of Interest.

Accreditation

John Wiley and Sons, Inc. is accredited by the Accreditation Council for Continuing Medical Education to provide continuing medical education for physicians.

John Wiley and Sons, Inc. designates this journal-based CME activity for a maximum of 1.0 *AMA PRA Category 1 Credit*TM. Physicians should only claim credit commensurate with the extent of their participation in the activity.

For information on applicability and acceptance of continuing medical education credit for this activity, please consult your professional licensing board.

This activity is designed to be completed within 1 hour. To successfully earn credit, participants must complete the activity during the valid credit period, which is up to two years from initial publication. Additionally, up to 3 attempts and a score of 70% or better is needed to pass the post test.

View this article online at wileyonlinelibrary.com. DOI: 10.1002/jmri.26058

Received Feb 5, 2018, Accepted for publication Mar 26, 2018.

*Address reprint requests to: V.G., Department of Radiology, Level 1, Lambeth Wing, St Thomas' Hospital, Westminster Bridge Road, London SE1 7EH, UK. E-mail: vicky.goh@kcl.ac.uk

From the ¹Biomedical Engineering, School of Biomedical Engineering & Imaging Sciences, King's Health Partners, St Thomas' Hospital, London, UK; ²Cancer Imaging, School of Biomedical Engineering & Imaging Sciences, King's College London, King's Health Partners, St Thomas' Hospital, London, UK; ³Radiology, Guy's & St Thomas' NHS Foundation Trust, London, UK; and ⁴MR Research Collaborations, Siemens Healthcare, Frimley, UK.

This is an open access article under the terms of the Creative Commons Attribution License, which permits use, distribution and reproduction in any medium, provided the original work is properly cited.

Cancer remains a global killer alongside cardiovascular disease. A better understanding of cancer biology has transformed its management with an increasing emphasis on a personalized approach, so-called "precision cancer medicine." Imaging has a key role to play in the management of cancer patients. Imaging biomarkers that objectively inform on tumor biology, the tumor environment, and tumor changes in response to an intervention complement genomic and molecular diagnostics. In this review we describe the key principles for imaging biomarker development and discuss the current status with respect to magnetic resonance imaging (MRI).

Level of Evidence: 5

Technical Efficacy: Stage 5

J. MAGN. RESON. IMAGING 2018;48:13–26.

Cancer affects 14.1 million new patients yearly and is the second most common killer disease worldwide.¹ Clinicians have long recognized that cancer represents a very heterogeneous disease. Patients with the same clinical presentation, tumor type, and stage may respond very differently to the same therapies and have different oncological outcomes. A better understanding of the extent of the genomic and molecular heterogeneity within cancers, as demonstrated in renal cell cancer,² has led to a refocusing of clinical management in recent years from a global to a more targeted approach.³ Currently, cancer therapies aim to be personalized to the patient's cancer, either to cure where there is limited disease, or to extend progression-free survival (PFS) where disease is advanced, yet maintaining a good quality of life, so-called "precision cancer medicine."

The US Food and Administration (FDA) approval of bevacizumab in 2004 for first-line metastatic colorectal cancer, after a Phase III trial demonstrated an improvement in median PFS of 4 months,⁴ has paved the way for an increasing number of licensed molecular targeted therapies. These include targeted HER-2 (human epidermal growth factor receptor 2) therapy (trastuzumab) for HER-2 overexpressing breast cancer and gastric/gastroesophageal cancer; targeted EGFR (epidermal growth factor receptor) therapy (cetuximab) for RAS wildtype colorectal cancer; targeted EGFR therapy (gefitinib or erlotinib) for EGFR mutated nonsmall-cell lung cancer; crizotinib for ALK (anaplastic lymphoma kinase) gene rearrangement nonsmall-cell lung cancer (present in ~5% of adenocarcinomas); and multikinase inhibitors (pazopanib, sorafenib, sunitinib) or mammalian target of rapamycin (mTOR) inhibitors (everolimus) for advanced renal cell cancer.

Trials of these therapies have highlighted the need for better diagnostics to support patient stratification for therapy as well as a rethink of how we gather evidence for novel therapeutics that may only work for a subgroup of patients. There has been burgeoning development of precision diagnostics as a consequence. For single agents targeted to clearly defined genetic "driver" alterations, companion diagnostics improve the selection of patients for therapy, eg, HER-2 expression to guide trastuzumab therapy and O⁶-methylguanine-DNA-methyltransferase (MGMT) methylation to guide temozolomide therapy. There has also been increasing interest in genomic analysis to guide therapy with

the move from single to multiagent regimens and also to improve prognostication, eg, oncoPrint DX in breast cancer that predicts the likelihood of recurrence from a 21-gene signature as well as the likelihood of response to chemotherapy.

While the advantages of genomic analysis and molecular analysis to improve patient stratification and to assist drug development is clear, in practice there have been continuing challenges to implementation. Some putative biomarkers may be invalid, as shown with EGFR expression for cetuximab.⁵ Cancers are also temporally and spatially heterogeneous, ie, a biopsy or assay may only reflect a moment in time, or one of a number of lesions. This plasticity has been a reason for mixed responses to therapies and the development of therapy resistance during previously effective targeted therapy.⁶ There may also be issues such as suboptimal methodology, challenging assays, validation, regulatory issues, and governance or cost that are a challenge for multicenter clinical trials.

Imaging still has an important role to play in personalized cancer medicine.⁷ Imaging is performed widely for the detection and characterization of cancer, for staging, for monitoring therapy, for detecting disease recurrence, or surveillance; imaging biomarkers hold great potential for optimizing patient care. The role of magnetic resonance imaging (MRI) has evolved within oncological practice in recent years. Previously reserved as an adjunctive problem-solving tool, the primary use of MRI has increased, such that MRI is now the primary imaging assessment tool for many cancers and plays an important part in management decisions. It is the initial imaging modality for diagnosing prostate cancer and myeloma; for staging rectal, cervical, and endometrial cancer; and for response assessment in hepatocellular cancer. In this review we will describe what constitutes an imaging biomarker, the principles of imaging biomarker development, and the current status of imaging biomarkers with respect to MRI.

What Constitutes a Biomarker?

The term "biomarker" refers to a characteristic that is measured objectively, as an indicator of normal biological processes, pathological changes, or response to an intervention.⁸ It includes molecular, histologic, radiographic, or physiologic characteristics. In terms of imaging, this may include

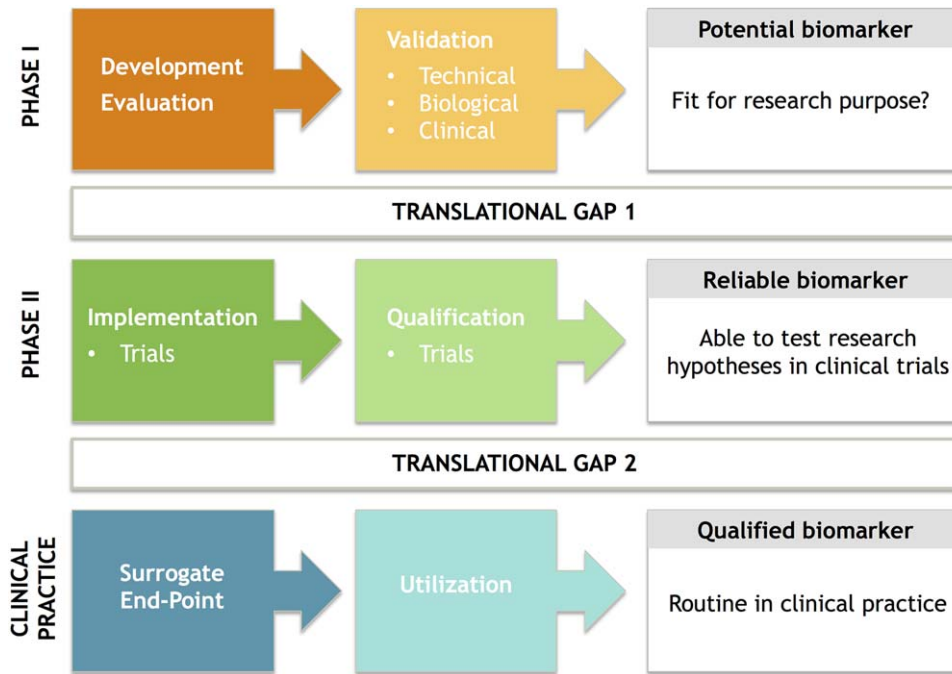


FIGURE 1: Schema highlighting steps taken in developing a potential imaging biomarker

anatomical, functional, and molecular characteristics.⁷ The advantages of imaging are its versatility, its widespread use, its relatively noninvasive nature (facilitating whole body imaging as well as longitudinal studies in individuals, thus capturing spatial and temporal heterogeneity), and its inherently quantitative nature. Imaging biomarkers may reflect a general cancer hallmark, eg, proliferation, metabolism, angiogenesis, apoptosis; specific molecular interactions; or agnostic features.⁹ Imaging biomarkers in cancer patients include biomarkers for detection (the identification of disease), prediction (the prediction of risk of disease or therapeutic outcome), prognostication (the prediction of oncological outcome), and response assessment (the evaluation of change with therapy). A number of imaging biomarkers are well established in clinical practice. Examples include staging with the American Joint Committee on Cancer (AJCC) TNM (tumor, node, metastasis) staging system (a prognostic biomarker) and objective response assessment by RECIST (Response Evaluation in Solid Tumors)¹⁰ in clinical trials (a response biomarker).

Imaging Biomarkers: From Discovery to Clinical Practice

For new potential imaging biomarkers several steps, often in parallel and complementary to each other, need to be undertaken for translation into clinical practice. These can be divided into the following phases following discovery: development and evaluation, validation, implementation, qualification, and utilization, essentially crossing two main translational gaps, translation into patients and translation into practice (Fig. 1).

In the initial phase, including development, evaluation, and validation, the aim is to ensure that the potential biomarker is robust and fit for purpose. Technical validation includes assessment of accuracy, precision, repeatability, and reproducibility across single and multiple centers; biological and clinical validation ensure that the biomarkers are linked to tumor biology, outcome variables, and thus of actual value in guiding decision-making in patients. During this phase, initial health economic analysis may also be undertaken to identify if there are cost barriers to implementation. Once the biomarker is established, it should be reliable enough to be implemented in clinical trials to test research hypotheses.

During the next phase, qualification of the biomarker may also be undertaken in large prospective trials. Qualification aims to confirm that the biomarker is associated with the clinical endpoint of interest and aims to demonstrate cost effectiveness and health impact. This supportive evidence is key to the translation into clinical practice and widespread utilization. Key recommendations have been proposed in a recent consensus article.¹¹

Advantages of MRI as an Imaging Biomarker

Ideally, there are a number of characteristics an imaging biomarker should have (Table 1). MRI has many advantages, including its superior soft-tissue contrast, high spatial resolution; its ability to obtain multiple contrasts in a single examination; and its ability to assess physiology, eg, vascularization, oxygenation, and diffusion. Assessment of the molecular environment is also achievable, albeit at a lower sensitivity compared to positron emission tomography

TABLE 1. Key Characteristics and Challenges for MRI Biomarkers

Characteristics	Challenges for MRI	Developments
Sensitive	Signal to noise ratio (SNR) Contrast to noise ratio (CNR) Spatial resolution Artifacts	New sequences
Specific & biologically relevant	Targeted versus physiological or morphological imaging	Evaluation of more targeted imaging, eg, receptor imaging, targeted nanoparticles
Robust	Variance among imaging systems, manufacturers & practice	Multivendor & multicenter involvement to standardize data acquisition, reconstruction & analysis
Quantifiable & reproducible	Variance among imaging systems, manufacturers & practice	Advanced acquisition and reconstruction to exploit data redundancy Single-sequence MRI to acquire several image contrasts in a coregistered fashion, eg, MR fingerprinting
Cost effective	Higher cost compared to computed tomography (CT) or ultrasound (US)	Reduction in scanner time with faster acquisitions

(PET). A number of MRI biomarkers are already established or well on their way to being established in clinical practice for oncological assessments (Table 2). These include BI-RADS (Breast Imaging Reporting and Data System),¹² LI-RADS (Liver Imaging Reporting and Data System),^{13,14} and PI-RADS (Prostate Imaging Reporting and Data System)¹⁵ for the diagnosis of breast, hepatocellular cancers, and prostate, respectively, in addition to TNM staging and RECIST response evaluation. Quantitative biomarkers that have crossed the first translational gap and are being used to test hypotheses in research studies and clinical trials include vascular parameters such as initial area under the gadolinium curve (iAUGC) or transfer constant (K^{trans}) from dynamic gadolinium enhanced (DCE) contrast imaging and apparent diffusion coefficient (ADC) from diffusion-weighted MRI (Table 2).

Morphology-Based MRI Biomarkers

Current morphology-based cancer biomarkers utilize the multiple contrasts and high spatial resolution of MRI. T_2 -weighted and T_1 -weighted sequences are part of every cancer protocol. T_2 -weighting highlights structures with a longer T_2 relaxation time. Thus, organs with a high water content, eg, bladder, appear of high signal on T_2 -weighted imaging, while cancers typically appear of intermediate signal. T_2 -weighted image contrast is encoded by a long echo time (TE) and long repetition time (TR). Typically, 2D imaging is performed in axial, sagittal, and/or coronal planes using a fast/turbo spin echo sequence. 3D imaging can be

performed using a 3D T_2 w-TSE with optimized flip angle evolution along the echo train (eg, Siemens SPACE, Philips VISTA, GE CUBE). T_1 -weighting highlights structures with a short T_1 , eg, fat, melanin. T_1 -weighted image contrast is encoded by a short TE and short TR. T_1 w-MRI is acquired with fast gradient echo sequences in 2D (Siemens FLASH, Phillips FFE, GE GRE) or 3D (Siemens VIBE, Philips THRIVE, GE Lava).

Diagnostic Biomarker

A key example of a recently established diagnostic biomarker is PI-RADS in suspected prostate cancer, currently on version 2.0,¹⁵ utilizing multiparametric MRI. The PROMIS trial^{16,17} has recently published its findings confirming a role for multiparametric MRI in the diagnostic pathway of patients with suspected prostate cancer. This enrolled 740 men, 576 of whom underwent 1.5T multiparametric MRI followed by both transrectal ultrasound (TRUS) biopsy and template prostate mapping biopsy. On template prostate mapping biopsy, 408 (71%) of 576 men had cancer with 230 (40%); of 576 patients it was clinically significant. For clinically significant cancer, multiparametric MRI was more sensitive (93%, 95% confidence interval [CI] 88–96%) than TRUS biopsy (48%, 42–55%; $P < 0.0001$). Using multiparametric MRI to triage men might allow 27% of patients to avoid a primary biopsy and improve detection of clinically significant cancer. Using a structured reporting scheme such as PI-RADS standardizes practice, provides an objective score of the likelihood of disease, and helps direct targeted biopsy. Risk scores to assess the likelihood of clinically significant cancer are

TABLE 2. Established and Validated MRI Biomarkers in Clinical Use

Biomarker	Characteristic	MRI sequence
Established biomarkers in clinical practice		
Detection & characterization		
BI-RADS (Breast Imaging Reporting and Data System) PI-RADS (Prostate Imaging Reporting and Data System) LI-RADS (Liver Imaging Reporting and Data System)	Lesion morphology	T2-weighted, T1-weighted, diffusion weighted, postcontrast-enhanced imaging
Curve shape	Degree of vascularization	Dynamic T1-weighted imaging following intravenous injection of gadolinium-based contrast agent
Staging		
TNM stage	Tumor morphology, presence of nodes, and metastases	T2-weighted, T1-weighted imaging \pm diffusion weighted, postcontrast-enhanced imaging
Response		
RECIST (Response Evaluation Criteria In Solid Tumors)	Change in tumor size	T2-weighted imaging
Validated biomarkers in clinical cancer research		
Apparent diffusion coefficient (ADC)	Cellularity	Diffusion-weighted imaging, at least 2 b-values
Initial area under the gadolinium curve (iAUGC) Transfer constant (K^{trans})	Perfusion Permeability	Dynamic T1-weighted imaging following intravenous injection of gadolinium-based contrast agent

defined as PI-RADS 1: very low, PI-RADS 2: low, PI-RADS 3: intermediate, PI-RADS 4: high, to PI-RADS 5: very high. A meta-analysis has revealed overall high sensitivity and specificity of 0.74 and 0.88, respectively, for prostate cancer detection with PI-RADS.^{18,19} MRI is performed with a multiparametric acquisition of at least T_2 -weighted and diffusion-

weighted sequences²⁰ (Fig. 2). This combines high resolution, high soft-tissue contrast of T_2 -weighted imaging with the diffusion-weighted imaging sensitivity for cancer.²¹ Additional dynamic contrast-enhanced sequences provide information of wash-in and wash-out characteristics and may provide additional diagnostic value. A recent study has demonstrated



FIGURE 2: Multiparametric prostate MRI demonstrates a left mid-gland PI-RADS 5 peripheral zone lesion extending beyond the prostate (a: T_2 -weighted, b: diffusion-weighted apparent diffusion coefficient map, c: arterial phase dynamic contrast-enhanced T_1 -weighted image).

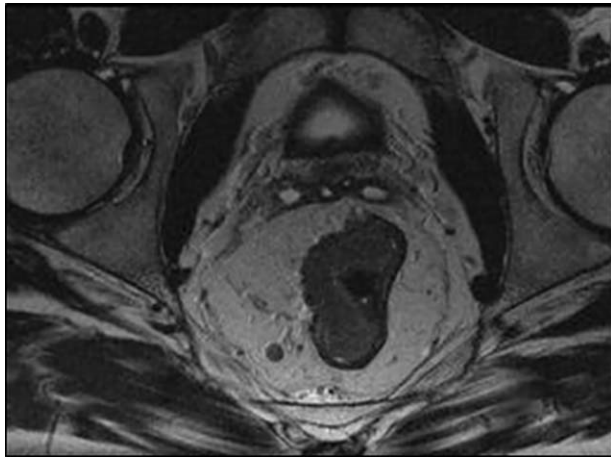


FIGURE 3: T₂-weighted axial image demonstrates a T3N1 rectal cancer extending beyond the rectal wall but not involving the potential resection margin

an increase in the probability of cancer detection of 16%, 16%, and 9% for PI-RADS category 2, 3, and 4 lesions, respectively, with DCE-MRI.²²

Prognostic Biomarker: Staging

Staging is an important imaging biomarker for patient stratification. MRI is the primary staging modality for a number of cancers including rectal cancer. In addition to TNM-Stage grouping, which provides an indication of relative 5-year overall survival (Stage I [localized, T1/2], node negative: 95%; vs. Stage IV [metastatic, any T,N]: 11%), MRI also has a predictive role in terms of likely involvement of the resection margin and PFS^{23–25} (Fig. 3).

Response Biomarker: RECIST

RECIST criteria provide a standardized, objective assessment of response to therapy in clinical trials.¹⁰ Classification of response is divided into four categories (complete response, partial response, stable disease, progressive disease) based on

size change of specified measurable target lesions (>1 cm) or nodes (>1.5 cm short axis) (Table 3). From a regulatory perspective, RECIST remains the key response biomarker in clinical trials and is used as a surrogate endpoint.

Validated MRI Biomarkers Requiring Qualification

Diffusion-Weighted MRI

ADC is a biomarker that has crossed the first translational gap and is used to test research hypotheses in clinical trials.²⁶ The biophysical basis of diffusion-weighted imaging is the microscopic displacement of water molecules ($\Delta x \approx 30 \mu\text{m}$ in $\Delta t = 50 \text{ msec}$) due to thermal Brownian motion. In cancers the tumor environment restricts this motion, thus a measurement of the effective displacement, the ADC, gives important microscopic information. Tumor ADC from b-values less than 1000 s/mm^2 effectively provide a measure of the extracellular space; although cell size, cell arrangements, cell density, integrity of cell membranes, glandular structures, extracellular space viscosity, and tortuosity will influence this measurement. Studies have correlated ADC with histological grade in a number of cancers.^{27–30}

The diffusion image contrast is encoded by using a gradient pair (Stejskal-Tanner gradient²⁶), which can be either a bipolar gradient pair in gradient echo or the same polarity in spin echo. This gradient causes a change in the resonant Larmor frequency of a spin isochromat, leading to the following phase accumulation ϕ :

$$\phi = \int_0^t \Delta\omega dt' = \gamma \int_0^t \vec{G}(t') \cdot \vec{r}(t') dt'$$

where \vec{G} is the applied gradient waveform applied for a duration t , \vec{r} is the spatial position of the spin

TABLE 3. Response Categorization Based on Changes in Target and Nontarget Lesions

RECIST		
Categorization	Target lesions	Nontarget lesions
Complete response (CR)	Disappearance of all target lesions (TL). All nodes <10 mm, ie, nonpathological	Disappearance of all nontarget lesions. All nodes <10 mm, ie, nonpathological
Partial response (PR) Stable disease (SD)	>30% decrease in the sum of TL diameters Neither PR nor PD	Non CR/PD: Persistence of ≥ 1 nontarget lesion
Progressive disease (PD)	>20% increase in the sum of TL diameters. Absolute increase of at least 5 mm. New lesions	Unequivocal progression of existing nontarget lesions New lesions

Target lesions: Up to 5 measured, 2 maximum per organ.

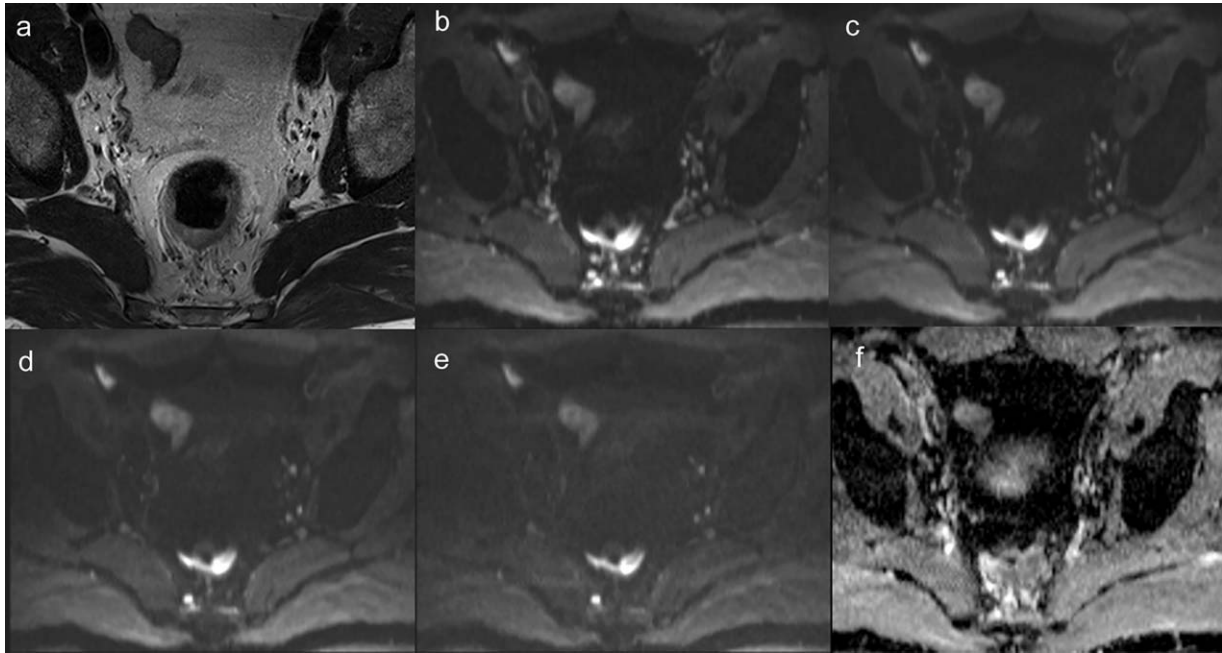


FIGURE 4: The T_2 axial oblique image (a) of a rectal cancer, diffusion-weighted images with increasing b-weighting 0 (b), 100 (c), 500 (d), and 800 s/mm^2 (e), and corresponding ADC_{0-800} map (f) is shown. Signal loss is demonstrated within the rectal cancer with increasing b-weighting. The signal loss is greater for normal tissue than for the cancer.

isochromat, and γ the gyromagnetic ratio. Thus, spins, which move during the application of the gradient pair, will not be properly rephased. This loss in phase coherence secondary to spatial displacement causes a reduction in the signal. For random spin diffusion motion in an image voxel, this signal cancellation is related to the variance of the Gaussian phase distribution $\langle \phi^2 \rangle$ and the product bD :

$$S = S_0 e^{-\langle \phi^2 \rangle} = S_0 e^{-bD}$$

Where S is the diffusion-weighted signal and S_0 is the signal without diffusion weighting.

Thus, the degree of attenuation depends on the dimensionless product of the diffusion coefficient D (in mm^2/sec) and the b-value (in sec/mm^2). The b-value is used to control the diffusion-weighted contrast with higher diffusion weighting at higher b-values. Typically, b-values of 0–1500 s/mm^2 are applied in clinical practice and ADC is obtained from monoexponential fitting of the signal loss (Fig. 4). In practice, other factors contribute to signal loss including T_2 -relaxation and bulk motion. In a given voxel, ADC will reflect the relative contribution of the different compartments.

A number of studies have evaluated ADC as a response biomarker in a number of tumor types across different therapies in research studies including the multicenter setting. These studies have shown that a common pattern is an increase in ADC_{mean} to a varying extent with different therapies. This may occur within days of starting treatment; a higher change in ADC_{mean} is also associated with a pathological good response.^{31–39}

The variability of ADC in clinical studies has been reported to be relatively low at $\leq 15\%$ ⁴⁰ and in ice-water phantom studies as low as 3%.⁴¹ Nevertheless, there are considerations to be made in the trial setting⁴² and technical challenges to acquiring robust diffusion-weighted biomarkers and qualification as a biomarker.²⁶ TR should be sufficiently long to avoid underestimation of ADC due to T_1 saturation effect; TE should be minimized to achieve better signal-to-noise ratio (SNR), to minimize motion and susceptibility artifacts. Good fat suppression is required to minimize ghosting artifacts; short tau inversion recovery (STIR) may be preferred to spectral presaturation attenuated by inversion recovery (SPAIR) or chemical shift selective water-only excitation techniques, where a large field of view is necessary at 1.5T, as STIR is less sensitive to B0 field inhomogeneities. Geometric distortion and susceptibility artifacts caused by eddy currents related to EPI may be improved by shortening the echo train length, eg, through adapting the receiver bandwidth to reduce the echo spacing, use of parallel imaging, zoomed excitation, or readout segmented imaging.

Dynamic Contrast-Enhanced MRI

DCE MRI refers to the rapid acquisition of a time series of T_1w images before, during, and after intravenous administration of a gadolinium-based contrast agent. Gadolinium contrast agents are small hydrophilic molecules with a short circulation half-life, typically < 1 hour. These contrast agents shorten the T_1 -relaxation rate, and thus cause signal enhancement related to the delivery and leakage rate of

contrast agent within the tissue of interest, providing a surrogate measure of angiogenesis.

While qualitative assessment of curve shape is an established imaging biomarker, eg, for the evaluation of suspected breast and prostate cancer, the use of quantitative vascular parameters remains in the domain of clinical trials. In terms of qualitative assessment, three distinct curve shapes are recognized: Type 1) slow rising enhancement (benign); Type 2) rapid enhancement with a plateau (may be malignant); and Type 3) rapid enhancement followed by rapid washout (malignant).

For assessing quantitative parameters, baseline T_1 mapping is required usually with a dual flip angle 3D T_1 -weighted spoiled gradient recalled echo acquisition (e.g., $2^\circ/18^\circ$) with other parameters remaining constant.

The baseline T_1 value (T_{10}) is estimated from fitting the signal intensity of the images acquired with different flip angles to the following equation:

$$S = \frac{S_0(1-E_1)\sin(\alpha)}{1-E_1\cos(\alpha)}$$

where S is acquired T_1 -weighted signal, α represents the applied flip angle in each acquisition, S_0 is the T_1 fully relaxed signal, and $E_1 = e^{-\frac{TR}{T_{10}}}$, where TR is the sequence repetition time. Contrast agent administration, typically 0.1 mmol/kg body weight, is followed by a dynamic acquisition for up to 5 minutes with a temporal resolution on the order of 3–5 seconds between acquisitions. Contrast agent concentration may be estimated with the following equation:

$$\frac{1}{T_1(t)} = \frac{1}{T_{10}} + r_1 C$$

where $T_1(t)$ represents the T_1 change over time due to the contrast agent, T_{10} represents the T_1 of the tissue at baseline, r_1 represents the T_1 relaxivity of the contrast agent, and C represents the unknown contrast concentration.

The Tofts and Kermode model⁴³ is applied most commonly to determine K^{trans} (a product of flow and transfer permeability):

$$\frac{dC_t(t)}{dt} = K^{trans} C_p(t) - k_{ep} C_t(t)$$

where $C_t(t)$ and $C_p(t)$ represent the contrast agent concentration in tissue and plasma as a function of time, respectively, K^{trans} represents transfer constant, k_{ep} represents the rate constant; or as an extended model to account for the contrast agent in the vasculature, when vascular volume cannot be neglected.

$$C_t(t) = v_p C_p(t) + K^{trans} \int_0^t C_p(t') \exp\left(\frac{-K^{trans}(t-t')}{v_e}\right) dt'$$

where $C_t(t)$ and $C_p(t)$ represent the contrast agent concentration in tissue and plasma, respectively, K^{trans} represents

transfer constant, k_{ep} represents the rate constant; v_p represent the fractional plasma volume; and v_e the fractional extracellular extravascular volume.

In the last 15 years, over 110 studies in 2268 patients have utilized quantitative DCE-MRI as a biomarker in clinical studies and trials reflecting the use of DCE-MRI to assess vascular activity in drug development,⁴⁴ in particular to assess the effect of antiangiogenic or antivascular therapy (Fig. 5). Consistent reduction in the initial area under the gadolinium curve (iAUGC) and K^{trans} have been found for a number of therapies including VEGF-targeted agents (bevacizumab) and multikinase inhibitors (pazopanib, sunitinib, sorafenib), as early as a few hours after dosing.

Nevertheless, the variability of K^{trans} in clinical studies remains a major issue (>50%), and baseline reproducibility has been utilized in clinical trials on an individual basis in order to be able to determine whether the measured change is related to therapeutic effect. Accurate determination of the arterial input function (AIF), which characterizes contrast agent arrival in a feeding blood vessel within the tumor, remains a challenge to accurate quantification. As an alternative to subject-specific direct measurement of AIF (subject to flow artifacts, nonlinear effects of high contrast agent concentrations, and partial volume effects), population-based AIFs⁴⁵ or reference tissue-based methods⁴⁶ have been advocated. Accurate T_1 -mapping also remains a challenge, as B1 inhomogeneity, particularly at 3T and higher field strengths, limit the accuracy of T_1 -estimates derived from the typically employed variable flip angle technique. Recent developments propose to include B1+ for T_1 -mapping.⁴⁷ To overcome the challenge of achieving both high spatial and temporal resolution for the DCE data acquisition, advanced methods have been proposed, such as combining parallel imaging, compressed sensing and non-Cartesian sampling,⁴⁸ view sharing,⁴⁹ and motion compensation.⁵⁰

Emerging MRI Biomarkers

Further emerging quantitative biomarkers are undergoing evaluation (Table 4), related to the following techniques: intravoxel incoherent motion (IVIM), diffusion kurtosis imaging, blood and tissue oxygenation level-dependent MRI (BOLD/TOLD), MR elastography, and relaxometry imaging. There has also been growing interest in extracting additional agnostic features from standard and quantitative MRI sequences, so-called radiomics.⁹

Pseudodiffusion and Intravoxel Incoherent Motion

Bulk water motion in capillaries can also cause phase dispersion in diffusion-weighted MRI.^{51,52} The loss in signal is similar to that seen with true diffusion and more marked at low b-values. Diffusion-weighted MRI always measures both, but the relative contribution depends on the choice of

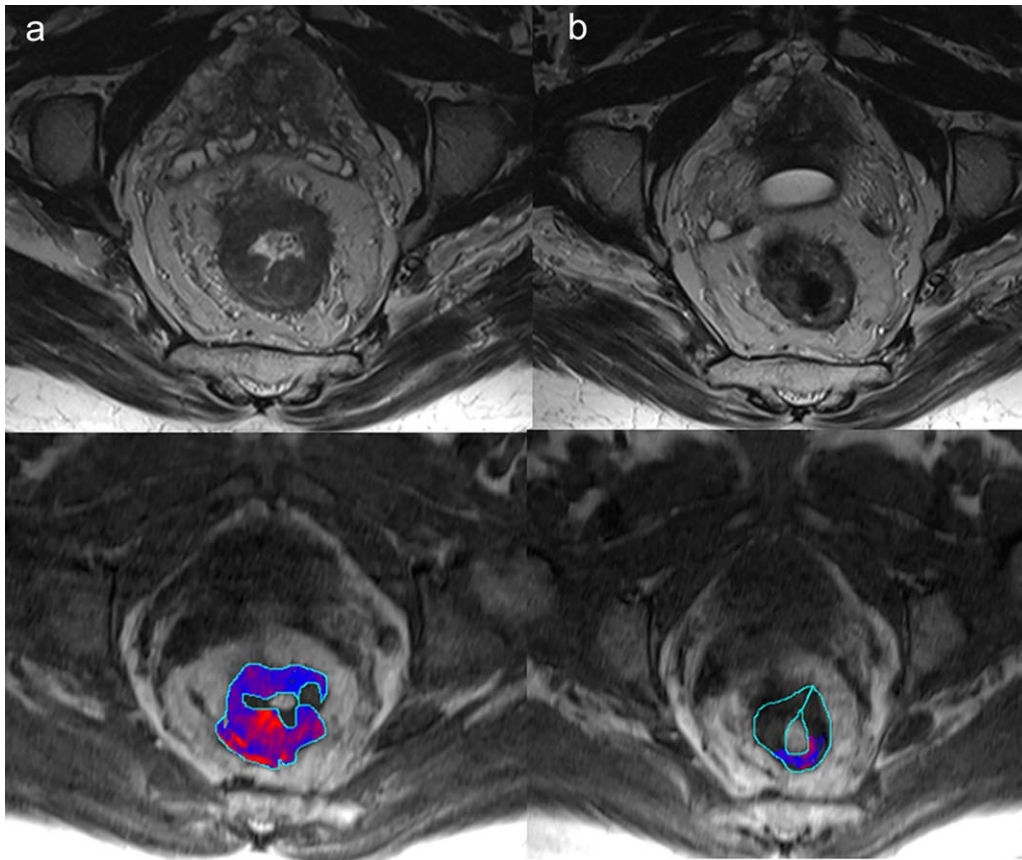


FIGURE 5: T₂-weighted (a) and corresponding transfer constant maps (K^{trans} , b) before and after three cycles of therapy with an antiangiogenic and triplet chemotherapy. A decrease in tumor vascularization is noted following three cycles of therapy.

b-values. The contribution of true diffusion and perfusion towards signal loss can be defined as follows:

$$S(b) = (1 - f_v) e^{-bD} + f_v e^{-bD^*}$$

where S is the acquired diffusion-weighted signal, b represents the b-value, f_v represents the fractional volume of flowing water molecules within capillaries; $(1 - f_v)$ is the fraction of molecules undergoing true diffusion; D represents tissue

TABLE 4. Emerging Biomarkers Undergoing Validation in Research Studies

Emerging biomarkers	Measure/biological correlate	MRI sequence
f , D^*	Pseudoperfusion	Multiple low b-value diffusion weighted imaging (intravoxel incoherent motion, IVIM)
Kurtosis (K_{app})	Microstructural complexity	Diffusion kurtosis imaging (DKI)
$R2^*$ $R1$ $\Delta R2^*$ $\Delta R1$	Relaxation rate Oxygenation	Blood oxygenation level dependent imaging (BOLD) Tissue oxygenation level dependent imaging (TOLD) \pm oxygen/carbogen challenge
Elasticity Viscosity	Tissue mechanics and viscoelastic parameters	Elastography: motion sensitive sequence to encode shear wave propagation
Specific metabolites, eg, Choline	Metabolite concentration	Spectroscopy
T1 T2	Relaxation time Microenvironment	Multiecho relaxometry imaging
Texture features	Heterogeneity	Any

diffusion coefficient and D^* the pseudodiffusion coefficient. D^* the pseudodiffusion coefficient associated with blood flow is about $10 \times 10^{-3} \text{ mm}^2/\text{sec}$ in the brain and $70 \times 10^{-3} \text{ mm}^2/\text{sec}$ in the liver compared to D , which is $1 \times 10^{-3} \text{ mm}^2/\text{sec}$.

Assessing f_v and D^* may be feasible for patients with poor renal function, an allergy precluding intravenous administration of contrast agent, or at high risk of developing nephrogenic systemic fibrosis.⁵³

However, one of the issues highlighted to date is the poor test–retest variability of f and D^* ,⁵⁴ on the order of $>100\%$ in some cancers, eg, rectal.⁵⁵ There also appears some contention as to technical/biological correlates: while some studies have shown a relationship between IVIM and DCE-MRI parameters,^{56–58} others have not in some cancers, eg, hepatocellular carcinoma.⁵⁹ One also has to be aware that flow from glandular secretions, eg, pancreas, may be difficult to separate from micro-capillary perfusion. A potential application is as a diagnostic biomarker, where current characterization may be a challenge, eg, pancreas.^{60,61}

Apparent Diffusional Kurtosis

Diffusion kurtosis imaging characterizes non-Gaussian diffusion behavior at high b-values ranging from 1000–3000 sec/mm^2 . A polynomial decay model is fitted to an acquisition using at least three b-values to obtain D_{app} and K_{app} representing the heterogeneity of the cellular microstructure. The diffusion signal S_i for a given b-value b_i is given by:

$$S_i = S_0^* e^{b_i D_{app} + \frac{1}{6} D_{app}^2 b_i^2 K_{app}}$$

where S_0 is the signal without diffusion weighting, K_{app} is the apparent diffusional kurtosis, and D_{app} is the diffusion coefficient. K_{app} reflects the signal curvature away from a monoexponential fit. The rationale proposed for assessing kurtosis is that it may better reflect the tumor intracellular microstructure,^{62,63} although it will also be influenced by extracellular properties. Higher kurtosis may be noted where there are higher intracellular interfaces; for example, increased nuclear-cytoplasmic ratio of tumor cells.⁶⁴ Preliminary studies in prostate cancer have suggested potential as a diagnostic biomarker,⁶⁵ eg, to improve characterization (grading),^{66,67} although not all studies have confirmed additional advantages over monoexponential ADC.^{68,69} Studies have also suggested its potential as a response biomarker. A study in hepatocellular carcinoma has suggested that K_{app} performs better than ADC in detecting viable disease posttreatment.⁷⁰

Tumor Elasticity and Viscosity

Magnetic resonance elastography (MRE) quantifies the viscoelastic properties of tissue by assessing its elastic response to an applied force, similar to palpation in clinical practice. The applied force consists of harmonic mechanical waves, ranging typically between 20 and 80 Hz in frequency and

propagated into the human body by a vibrating transducer applied to the body surface. The consequent tissue motion is captured using rapid motion-sensitive MRI sequences. Through mathematical inversion algorithms, the local shear wave properties can be derived from the periodical variations in MRI signal; the local viscoelastic parameters (elasticity and viscosity) are then calculated using the complex shear modulus equation.⁷¹ The underpinning experimental observation for the application of MRE to cancer is that malignancy increases stiffness through collagen deposition in the extracellular matrix and raises interstitial pressure levels from its abnormal vasculature.⁷² MRE has shown promising potential for the characterization of focal lesions (benign vs. malignant) in multiple organs, including the liver,⁷³ breast,⁷⁴ pancreas,⁷⁵ and kidney.⁷⁶ It may also serve as a potential biomarker of treatment resistance.

Tumor Oxygenation

Tumor oxygenation may be measured indirectly by BOLD and TOLD-MRI techniques. With BOLD MRI, endogenous hemoglobin acts as a paramagnetic contrast agent that increases the transverse relaxation rate ($R2^*$) in blood and surrounding tissue. $R2^*$ is measured from multiple spoiled gradient recalled echo images with increasing echo times. $R2^*$ is calculated from the gradient of a straight line fitted to a plot of \ln -signal intensity to TE. Higher $R2^*$ reflects higher deoxy-hemoglobin levels and lower blood oxygenation. $R2^*$ may have a role as a response biomarker. One study has shown that $R2^*$ is inversely correlated to blood volume and increases in breast cancer treated with two cycles of neoadjuvant chemotherapy with greater changes in patients with pathological response.⁷⁷ However, BOLD measurements will be affected by the underlying tissue relaxivity and will be affected by hemorrhage and susceptibility artifacts.

With TOLD MRI the longitudinal relaxation rate ($R1$) is measured. $R1$ is sensitive to changes in the O_2 dissolved in blood plasma and interstitial fluid. When a hyperoxic gas is inhaled, the excess oxygen dissolved will result in a higher $R1$ value. A positive change in $R1$ will identify areas with fully saturated hemoglobin. Areas where there is no positive change in $R1$ may reflect regions of hypoxia, particularly if perfusion is present. Current approaches are focusing on the feasibility of combining $R2^*$ and $R1$ measurement with oxygen challenge to assess tumor oxygenation.⁷⁸

Quantitative MRI With or Without Exogenous Contrast agents

In current clinical practice, a diagnosis based on MRI primarily relies on the *qualitative* assessment of images. In contrast, *quantitative* measurements of tissue properties with or without endogenous contrast agents may provide more accurate and reproducible information. Without the use of exogenous contrast agents, relaxometry yields quantitative measurement

of intrinsic tissue relaxation times T_1 and T_2 ,^{79–82} T_2^* , proton density. In addition, important molecular information about tumor physiology and metabolism (“tumor micro-environment”) may be obtained from MR spectroscopy (MRS),^{83–88} chemical exchange saturation transfer imaging (CEST),⁸⁹ and amide proton transfer (APT).⁹⁰ Further, relaxometry with exogenous contrast agents enables imaging of perfusion, using either gadolinium-based contrast agents⁹¹ and dynamic T_1w (DCE), as discussed previously, or T_2^*w MRI (dynamic susceptibility contrast-enhanced [DSC]). Superparamagnetic iron oxide (SPIO) nanoparticles in combination with T_2w and T_2^*w MRI have been developed as imaging probes for targeted molecular MRI, cell tracking, and drug delivery (“theranostics”).^{92–94} Alternatively, highly specific, background-free imaging can be achieved via nonproton imaging using, eg, F-19^{95–97} or hyperpolarized agents C-13.^{98,99} However, these require hardware modifications to be able to image the nonproton frequencies.

Novel quantitative methods have also been proposed to acquire several tissue properties at once.^{100,101} A method termed “MR-fingerprinting” utilizes a (pseudo) randomized acquisition sequence to encode a tissue-specific “Fingerprint” into an MR time series signal.¹⁰² This has recently also been adapted and applied to cancer imaging.^{103–105}

Finally, to achieve its full potential, a key challenge of multiparametric MRI is standardization across multiple platforms, which involves the use of phantoms and careful review of implementation.¹⁰⁶

Radiomics

Radiomics is an evolving area in medical imaging whereby a large number of features are extracted and interpreted using bioinformatic approaches.^{9,107} The underlying rationale for radiomics lies in the supposed relationship between extracted image parameters and tumor molecular phenotype and/or genotype. It is known that genotypic heterogeneity contributes to divergent tumor biological behavior, including poor treatment response and a more aggressive phenotype. Therefore, there is growing interest in using imaging radiomic signatures either alone or in combination with other clinical or -omics data, eg, radiogenomics, to improve tumor phenotyping (prognostication), to allow tumor subregions with different biological characteristics that may contribute to treatment resistance to be identified/segmented for therapies, and for the prediction and evaluation of therapies. Radiomic studies have used a number of techniques including statistical methods (histogram; gray-level co-occurrence matrix [GLCM]; gray-level difference matrix [GLDM], run length matrix [RLM], gray level size zone matrix [GLSZM], and neighborhood gray tone difference matrix [NGTDM]) with or without Gaussian or Wavelet transformation; and fractal-based methods across different sequences including T_2 -weighted, diffusion-weighted, and

DCE sequences. Initial radiogenomic studies including MRI have been performed in breast cancer^{108–110} renal cell carcinoma¹¹¹ and glioma.^{112,113} Variable reproducibility has been shown across different classes of features¹¹⁴ and further validation work is still required for radiomic biomarkers.

Conclusion

- Precision cancer medicine remains a desirable goal for cancer care.
- MRI offers many advantages as a diagnostic, prognostic, predictive, or response biomarker in cancer given its capability of multiple contrast and multiparametric quantitative imaging.
- A key challenge remains to improve the efficiency of biomarker translation from discovery to implementation. Clinical translation for emerging biomarkers remains slow.
- To overcome issues regarding biomarker measurement variability across devices and across manufacturers, phantoms for quality assurance, standardization of protocols and availability of reference value databases has helped to facilitate this, alongside networks and alliances including the Quantitative Imaging Network (QIN) (<http://imaging.cancer.gov/informatics/qin>), the Quantitative Imaging Biomarker Alliance (QIBA) (<http://www.rsna.org/qiba/>); the Quantitative Imaging in Cancer: Connecting Cellular Processes to Therapy (QuIC-ConCePT) (<http://www.quic-concept.eu/>) consortium; and the American College of Radiology Imaging Network (ACRIN).
- With emerging machine-learning approaches, quantitative MRI biomarkers will no doubt continue to expand to meet new challenges in the personalized care of oncology patients.

Acknowledgments

The authors acknowledge support from the Department of Health via the National Institute for Health Research Comprehensive Biomedical Research Centre award to Guy’s & St Thomas’ NHS Foundation Trust in partnership with King’s College London and King’s College Hospital NHS Foundation Trust; from the King’s College London/University College London Comprehensive Cancer Imaging Centre funded by Cancer Research UK and Engineering and Physical Sciences Research Council (EPSRC) in association with the Medical Research Council and Department of Health (C1519/A16463); and Wellcome EPSRC Centre for Medical Engineering at King’s College London (WT 203148/Z/16/Z).

References

1. Globocan, 2012. www.globocan.iarc.fr
2. Gerlinger M, Rowan AJ, Horswell S, et al. Intratumor heterogeneity and branched evolution revealed by multiregion sequencing. *N Engl J Med* 2012;366:883–892.
3. Schilsky RL. Personalized medicine in oncology: the future is now. *Nat Rev Drug Discov* 2010;9:363–366.
4. Hurwitz H, Fehrenbacher L, Novotny W, et al. Bevacizumab plus irinotecan, fluorouracil, and leucovorin for metastatic colorectal cancer. *N Engl J Med* 2004;350:2335–2342.
5. Chung KY, Shia J, Kemeny NE, et al. Cetuximab shows activity in colorectal cancer patients with tumors that do not express the epidermal growth factor receptor by immunohistochemistry. *J Clin Oncol* 2005;23:1803–1810.
6. Misale S, Yaeger R, Hobor S, et al. Emergence of KRAS mutations and acquired resistance to anti-EGFR therapy in colorectal cancer. *Nature* 2012;486:532–536.
7. Medical imaging in personalised medicine: a white paper of the research committee of the European Society of Radiology (ESR). *Insights Imaging* 2015;6:141–155.
8. White paper on imaging biomarkers. *Insights Imaging* 2010;1:42–45.
9. Gillies RJ, Kinahan PE, Hricak H. Radiomics: images are more than pictures, they are data. *Radiology* 2016;278:563–577.
10. Eisenhauer EA, Therasse P, Bogaerts J, et al. New response evaluation criteria in solid tumours: revised RECIST guideline (version 1.1). *Eur J Cancer* 2009;45:228–247.
11. O'Connor JP, Aboagye EO, Adams JE, et al. Imaging biomarker roadmap for cancer studies. *Nat Rev Clin Oncol* 2017;14:169–86.
12. Mercado CL. BI-RADS update. *Radiol Clin N Am* 2014;52:481–487.
13. Tang A, Bashir MR, Corwin MT, et al. Evidence supporting LI-RADS major features for CT- and MR imaging-based diagnosis of hepatocellular carcinoma: a systematic review. *Radiology* 2018;286:29–48.
14. Mitchell DG, Bruix J, Sherman M, Sirlin CB. LI-RADS (Liver Imaging Reporting and Data System): summary, discussion, and consensus of the LI-RADS Management Working Group and future directions. *Hepatology* 2015;61:1056–1065.
15. Weinreb JC, Barentsz JO, Choyke PL, et al. PI-RADS Prostate Imaging — Reporting and Data System: 2015, Version 2. *Eur Radiol* 2016;69:16–40.
16. El-Shater Bosaily A, Parker C, Brown LC, et al. PROMIS—Prostate MR imaging study: A paired validating cohort study evaluating the role of multiparametric MRI in men with clinical suspicion of prostate cancer. *Contemp Clin Trials* 2015;42:26–40.
17. Ahmed HU, El-Shater Bosaily A, Brown LC, et al. Diagnostic accuracy of multiparametric MRI and TRUS biopsy in prostate cancer (PROMIS): a paired validating confirmatory study. *Lancet* 2017;389:815–822.
18. de Rooij M, Hamoen EH, Futterer JJ, Barentsz JO, Rovers MM. Accuracy of multiparametric MRI for prostate cancer detection: a meta-analysis. *AJR Am J Roentgenol* 2014;202:343–351.
19. Hamoen EH, de Rooij M, Witjes JA, Barentsz JO, Rovers MM. Use of the Prostate Imaging Reporting and Data System (PI-RADS) for prostate cancer detection with multiparametric magnetic resonance imaging: a diagnostic meta-analysis. *Eur Radiol* 2015;67:1112–1121.
20. Kuhl CK, Bruhn R, Kramer N, Nebelung S, Heidenreich A, Schrading S. Abbreviated biparametric prostate MR imaging in men with elevated prostate-specific antigen. *Radiology* 2017;285:493–505.
21. Wu LM, Xu JR, Ye YQ, Lu Q, Hu JN. The clinical value of diffusion-weighted imaging in combination with T2-weighted imaging in diagnosing prostate carcinoma: a systematic review and meta-analysis. *AJR Am J Roentgenol* 2012;199:103–110.
22. Greer MD, Shih JH, Lay N, et al. Validation of the dominant sequence paradigm and role of dynamic contrast-enhanced imaging in PI-RADS version 2. *Radiology* 2017;285:859–869.
23. Beets-Tan RG, Beets GL, Vliegen RF, et al. Accuracy of magnetic resonance imaging in prediction of tumour-free resection margin in rectal cancer surgery. *Lancet* 2001;357:497–504.
24. Diagnostic accuracy of preoperative magnetic resonance imaging in predicting curative resection of rectal cancer: prospective observational study. *BMJ* 2006;333:779.
25. Taylor FG, Quirke P, Heald RJ, et al. Preoperative magnetic resonance imaging assessment of circumferential resection margin predicts disease-free survival and local recurrence: 5-year follow-up results of the MERCURY study. *J Clin Oncol* 2014;32:34–43.
26. Padhani AR, Liu G, Koh DM, et al. Diffusion-weighted magnetic resonance imaging as a cancer biomarker: consensus and recommendations. *Neoplasia* 2009;11:102–125.
27. Nakanishi M, Chuma M, Hige S, et al. Relationship between diffusion-weighted magnetic resonance imaging and histological tumor grading of hepatocellular carcinoma. *Ann Surg Oncol* 2012;19:1302–1309.
28. Winfield JM, Orton MR, Collins DJ, et al. Separation of type and grade in cervical tumours using non-mono-exponential models of diffusion-weighted MRI. *Eur Radiol* 2017;27:627–636.
29. Hotker AM, Mazaheri Y, Aras O, et al. Assessment of prostate cancer aggressiveness by use of the combination of quantitative DWI and dynamic contrast-enhanced MRI. *AJR Am J Roentgenol* 2016;206:756–763.
30. Kishimoto K, Tajima S, Maeda I, et al. Endometrial cancer: correlation of apparent diffusion coefficient (ADC) with tumor cellularity and tumor grade. *Acta Radiol* 2016;57:1021–1028.
31. Koh DM, Blackledge M, Collins DJ, et al. Reproducibility and changes in the apparent diffusion coefficients of solid tumours treated with combretastatin A4 phosphate and bevacizumab in a two-centre phase I clinical trial. *Eur Radiol* 2009;19:2728–2738.
32. Lee EM, Hong YS, Kim KP, et al. Phase II study of preoperative chemoradiation with S-1 plus oxaliplatin in patients with locally advanced rectal cancer. *Cancer Sci* 2013;104:111–115.
33. Sharma U, Danishad KK, Seenu V, Jagannathan NR. Longitudinal study of the assessment by MRI and diffusion-weighted imaging of tumor response in patients with locally advanced breast cancer undergoing neoadjuvant chemotherapy. *NMR Biomed* 2009;22:104–113.
34. Agarwal K, Sharma U, Sah RG, et al. Pre-operative assessment of residual disease in locally advanced breast cancer patients: A sequential study by quantitative diffusion weighted MRI as a function of therapy. *Magn Reson Imaging* 2017;42:88–94.
35. Cui Y, Zhang XP, Sun YS, Tang L, Shen L. Apparent diffusion coefficient: potential imaging biomarker for prediction and early detection of response to chemotherapy in hepatic metastases. *Radiology* 2008;248:894–900.
36. Reischauer C, Froehlich JM, Pless M, Binkert CA, Koh DM, Gutzeit A. Early treatment response in non-small cell lung cancer patients using diffusion-weighted imaging and functional diffusion maps—a feasibility study. *PLoS One* 2014;9:e108052.
37. Wong KH, Panek R, Welsh L, et al. The predictive value of early assessment after 1 cycle of induction chemotherapy with 18F-FDG PET/CT and diffusion-weighted MRI for response to radical chemoradiotherapy in head and neck squamous cell carcinoma. *J Nucl Med* 2016;57:1843–1850.
38. Harry VN, Semple SI, Gilbert FJ, Parkin DE. Diffusion-weighted magnetic resonance imaging in the early detection of response to chemoradiation in cervical cancer. *Gynecol Oncol* 2008;111:213–220.
39. Foltz WD, Wu A, Chung P, et al. Changes in apparent diffusion coefficient and T2 relaxation during radiotherapy for prostate cancer. *J Magn Reson Imaging* 2013;37:909–916.
40. Jafar MM, Parsai A, Miquel ME. Diffusion-weighted magnetic resonance imaging in cancer: Reported apparent diffusion coefficients, in-vitro and in-vivo reproducibility. *World J Radiol* 2016;8:21–49.
41. Malyarenko D, Galban CJ, Londy FJ, et al. Multi-system repeatability and reproducibility of apparent diffusion coefficient measurement

- using an ice-water phantom. *J Magn Reson Imaging* 2013;37:1238–1246.
42. deSouza NM, Winfield JM, Waterton JC, et al. Implementing diffusion-weighted MRI for body imaging in prospective multicentre trials: current considerations and future perspectives. *Eur Radiol* 2018; 28:1118–1131.
 43. Tofts PS, Brix G, Buckley DL, et al. Estimating kinetic parameters from dynamic contrast-enhanced T(1)-weighted MRI of a diffusable tracer: standardized quantities and symbols. *J Magn Reson Imaging* 1999;10: 223–232.
 44. Sung YS, Park B, Choi Y, et al. Dynamic contrast-enhanced MRI for oncology drug development. *J Magn Reson Imaging* 2016;44:251–264.
 45. Parker GJ, Roberts C, Macdonald A, et al. Experimentally-derived functional form for a population-averaged high-temporal-resolution arterial input function for dynamic contrast-enhanced MRI. *Magn Reson Med* 2006;56:993–1000.
 46. Kovar DA, Lewis M, Karczmar GS. A new method for imaging perfusion and contrast extraction fraction: input functions derived from reference tissues. *J Magn Reson Imaging* 1998;8:1126–1134.
 47. Sung K, Saranathan M, Daniel BL, Hargreaves BA. Simultaneous T1 and B1+ mapping using reference region variable flip angle imaging. *Magn Reson Med* 2013;70:954–961.
 48. Rosenkrantz AB, Geppert C, Grimm R, et al. Dynamic contrast-enhanced MRI of the prostate with high spatiotemporal resolution using compressed sensing, parallel imaging, and continuous golden-angle radial sampling: Preliminary experience. *J Magn Reson Imaging* 2015;41:1365–1373.
 49. Levine E, Daniel B, Vasanawala S, Hargreaves B, Saranathan M. 3D Cartesian MRI with compressed sensing and variable view sharing using complementary poisson-disc sampling. *Magn Reson Med* 2016; 1785:1774–1785
 50. Feng L, Axel L, Chandarana H, Block KT, Sodickson DK, Otazo R. XD-GRASP: Golden-angle radial MRI with reconstruction of extra motion-state dimensions using compressed sensing. *Magn Reson Med* 2016: 75:775–778.
 51. Le Bihan D, Breton E, Lallemand D, Aubin ML, Vignaud J, Laval-Jeantet M. Separation of diffusion and perfusion in intravoxel incoherent motion MR imaging. *Radiology* 1988;168:497–505.
 52. Le Bihan D. Intravoxel incoherent motion imaging using steady-state free precession. *Magn Reson Med* 1988;7:346–351.
 53. Iima M, Le Bihan D. Clinical intravoxel incoherent motion and diffusion MR imaging: past, present, and future. *Radiology* 2016;278:13–32.
 54. Andreou A, Koh DM, Collins DJ, et al. Measurement reproducibility of perfusion fraction and pseudodiffusion coefficient derived by intravoxel incoherent motion diffusion-weighted MR imaging in normal liver and metastases. *Eur Radiol* 2013;23:428–434.
 55. Sun H, Xu Y, Xu Q, Shi K, Wang W. Rectal cancer: Short-term reproducibility of intravoxel incoherent motion parameters in 3.0T magnetic resonance imaging. *Medicine* 2017;96:e6866.
 56. Lee EY, Hui ES, Chan KK, et al. Relationship between intravoxel incoherent motion diffusion-weighted MRI and dynamic contrast-enhanced MRI in tissue perfusion of cervical cancers. *J Magn Reson Imaging* 2015;42:454–459.
 57. Kim JH, Joo I, Kim TY, et al. Diffusion-related MRI parameters for assessing early treatment response of liver metastases to cytotoxic therapy in colorectal cancer. *AJR Am J Roentgenol* 2016;207:W26–32.
 58. Woo S, Lee JM, Yoon JH, Joo I, Han JK, Choi BI. Intravoxel incoherent motion diffusion-weighted MR imaging of hepatocellular carcinoma: correlation with enhancement degree and histologic grade. *Radiology* 2014;270:758–767.
 59. Hectors SJ, Wagner M, Besa C, et al. Intravoxel incoherent motion diffusion-weighted imaging of hepatocellular carcinoma: Is there a correlation with flow and perfusion metrics obtained with dynamic contrast-enhanced MRI? *J Magn Reson Imaging* 2016;44:856–864.
 60. Concia M, Sprinkart AM, Penner AH, et al. Diffusion-weighted magnetic resonance imaging of the pancreas: diagnostic benefit from an intravoxel incoherent motion model-based 3 b-value analysis. *Invest Radiol* 2014;49:93–100.
 61. Kang KM, Lee JM, Yoon JH, Kiefer B, Han JK, Choi BI. Intravoxel incoherent motion diffusion-weighted MR imaging for characterization of focal pancreatic lesions. *Radiology* 2014;270:444–453.
 62. Rosenkrantz AB, Padhani AR, Chenevert TL, et al. Body diffusion kurtosis imaging: Basic principles, applications, and considerations for clinical practice. *J Magn Reson Imaging* 2015;42:1190–1202.
 63. Le Bihan D. Apparent diffusion coefficient and beyond: what diffusion MR imaging can tell us about tissue structure. *Radiology* 2013;268: 318–322.
 64. Hectors SJ, Semaan S, Song C, et al. Advanced diffusion-weighted imaging modeling for prostate cancer characterization: correlation with quantitative histopathologic tumor tissue composition-A hypothesis-generating study. *Radiology* 2017:170904.
 65. Quentin M, Pentang G, Schimmoller L, et al. Feasibility of diffusional kurtosis tensor imaging in prostate MRI for the assessment of prostate cancer: preliminary results. *Magn Reson Imaging* 2014;32:880–885.
 66. Wang Q, Li H, Yan X, et al. Histogram analysis of diffusion kurtosis magnetic resonance imaging in differentiation of pathologic Gleason grade of prostate cancer. *Urol Oncol* 2015;33:337.e15–24.
 67. Tamura C, Shinmoto H, Soga S, et al. Diffusion kurtosis imaging study of prostate cancer: preliminary findings. *J Magn Reson Imaging* 2014; 40:723–729.
 68. Barrett T, McLean M, Priest AN, et al. Diagnostic evaluation of magnetization transfer and diffusion kurtosis imaging for prostate cancer detection in a re-biopsy population. *Eur Radiol* 2017 [Epub ahead of print].
 69. Roethke MC, Kuder TA, Kuru TH, et al. Evaluation of diffusion kurtosis imaging versus standard diffusion imaging for detection and grading of peripheral zone prostate cancer. *Invest Radiol* 2015;50:483–489.
 70. Goshima S, Kanematsu M, Noda Y, Kondo H, Watanabe H, Bae KT. Diffusion kurtosis imaging to assess response to treatment in hyper-vascular hepatocellular carcinoma. *AJR Am J Roentgenol* 2015;204: W543–549.
 71. Muthupillai R, Lomas DJ, Rossman PJ, Greenleaf JF, Manduca A, Ehman RL. Magnetic resonance elastography by direct visualization of propagating acoustic strain waves. *Science* 1995;269:1854–1857.
 72. Dvorak HF. Tumors: wounds that do not heal. Similarities between tumor stroma generation and wound healing. *N Engl J Med* 1986; 315:1650–1659.
 73. Garteiser P, Doblaz S, Daire JL, et al. MR elastography of liver tumours: value of viscoelastic properties for tumour characterization. *Eur Radiol* 2012;22:2169–2177.
 74. Sinkus R, Tanter M, Xydeas T, Catheline S, Bercoff J, Fink M. Viscoelastic shear properties of in vivo breast lesions measured by MR elastography. *Magn Reson Imaging* 2005;23:159–165.
 75. Shi Y, Gao F, Li Y, et al. Differentiation of benign and malignant solid pancreatic masses using magnetic resonance elastography with spin-echo echo planar imaging and three-dimensional inversion reconstruction: a prospective study. *Eur Radiol* 2017 [Epub ahead of print].
 76. Prezzi D, Neji R, Kelly-Morland C, et al. Characterization of small renal tumors with MR elastography. *Invest Radiol* (in press).
 77. Li SP, Taylor NJ, Makris A, et al. Primary human breast adenocarcinoma: imaging and histologic correlates of intrinsic susceptibility-weighted MR imaging before and during chemotherapy. *Radiology* 2010;257:643–652.
 78. Remmele S, Sprinkart AM, Muller A, et al. Dynamic and simultaneous MR measurement of R1 and R2* changes during respiratory challenges for the assessment of blood and tissue oxygenation. *Magn Reson Med* 2013;70:136–146.
 79. Liu W, Turkbey B, Senegas J, et al. Accelerated T2 mapping for characterization of prostate cancer. *Magn Reson Med* 2011;65:1400–1406.

80. Gibbs P, Liney GP, Pickles MD, Zelhof B, Rodrigues G, Turnbull LW. Correlation of ADC and T2 measurements with cell density in prostate cancer at 3.0 Tesla. *Invest Radiol* 2009;44:572–576.
81. Dregely I, Margolis DAJ, Sung K, et al. Rapid quantitative T2 mapping of the prostate using three-dimensional dual echo steady state MRI at 3T. *Magn Reson Med* 2016;76:1720–1729
82. Sabouri S, Chang SD, Savdie R, et al. Luminal water imaging: a new MR imaging T2 mapping technique for prostate cancer diagnosis. *Radiology* 2017;284:161687.
83. Evanochoko WT, Ng TC, Glickson JD. Application of in vivo NMR spectroscopy to cancer. *Magn Reson Med* 1984;1:508–534.
84. Bruhn H, Frahm J, Gyngell ML, et al. Noninvasive differentiation of tumors with use of localized H-1MR spectroscopy in vivo: initial experiments in patients with cerebral tumors. *Radiology* 1989;172:541–548.
85. Kurhanewicz J, Vigneron DB, Hricak H, Narayan P, Carroll P, Nelson SJ. Three-dimensional H-1 MR spectroscopic imaging of the in situ human prostate with high (0.24-0.7-cm³) spatial resolution. *Radiology* 1996;198:795–805.
86. Heerschap A, Jager GJ, van der Graaf M, et al. In vivo proton MR spectroscopy reveals altered metabolite content in malignant prostate tissue. *Anticancer Res* 1997;17:1455–1460.
87. Kurhanewicz J, Vigneron DB, Nelson SJ, et al. Citrate as an in vivo marker to discriminate prostate cancer from benign prostatic hyperplasia and normal prostate peripheral zone: detection via localized proton spectroscopy. *Urology* 1995;45:459–466
88. Scheidler J, Hricak H, Vigneron DB, et al. Prostate cancer: localization with three-dimensional proton MR spectroscopic imaging—clinico-pathologic study. *Radiology* 1999;213:473–480
89. Goffeney N, Bulte JW, Duyn J, Bryant LH Jr, van Zijl PC. Sensitive NMR detection of cationic-polymer-based gene delivery systems using saturation transfer via proton exchange. *J Am Chem Soc* 2001;123:8628–8629.
90. Zhou J, Payen JF, Wilson DA, Traystman RJ, van Zijl PC. Using the amide proton signals of intracellular proteins and peptides to detect pH effects in MRI. *Nat Med* 2003;9:1085–1090.
91. Weinmann HJ, Brasch RC, Press WR, Wesbey GE. Characteristics of gadolinium-DTPA complex: a potential NMR contrast agent. *AJR Am J Roentgenol* 1984;142:619–624
92. Qiao R, Yang C, Gao M. Superparamagnetic iron oxide nanoparticles: from preparations to in vivo MRI applications. *J Mater Chem* 2009;19:6274.
93. Li L, Jiang W, Luo K, et al. Superparamagnetic iron oxide nanoparticles as MRI contrast agents for non-invasive stem cell labeling and tracking. *Theranostics* 2013;3:595–615.
94. Korchinski DJ, Taha M, Yang R, Nathoo N, Dunn JF. Iron oxide as an MRI contrast agent for cell tracking. *Magn Reson Insights* 2015;8:15–29.
95. Mason RP, Rodbumrung W, Antich PP. Hexafluorobenzene: a sensitive ¹⁹F NMR indicator of tumor oxygenation. *NMR Biomed* 1996;9:125–134.
96. Diepart C, Magat J, Jordan BF, Gallez B. In vivo mapping of tumor oxygen consumption using ¹⁹F MRI relaxometry. *NMR Biomed* 2011;24:458–463.
97. McIntyre DJ, Howe FA, Ladroue C, Lofts F, Stubbs M, Griffiths JR. Can localised (¹⁹F) magnetic resonance spectroscopy pharmacokinetics of 5FU in colorectal metastases predict clinical response? *Cancer Chemother Pharmacol* 2011;68:29–36.
98. Gallagher FA, Kettunen MI, Day SE, et al. Magnetic resonance imaging of pH in vivo using hyperpolarized ¹³C-labelled bicarbonate. *Nature* 2008;453:940–943.
99. Day SE, Kettunen MI, Gallagher FA, et al. Detecting tumor response to treatment using hyperpolarized ¹³C magnetic resonance imaging and spectroscopy. *Nat Med* 2007;13:1382–1387.
100. Ding Y, Mason RP, McColl RW, et al. Simultaneous measurement of tissue oxygen level-dependent (TOLD) and blood oxygenation level-dependent (BOLD) effects in abdominal tissue oxygenation level studies. *J Magn Reson Imaging* 2013;38:1230–1236
101. Skorpil M, Brynolfsson P, Engström M. Motion corrected DWI with integrated T2-mapping for simultaneous estimation of ADC, T2-relaxation and perfusion in prostate cancer. *Magn Reson Imaging* 2017;39:162–167
102. Ma D, Gulani V, Seiberlich N, et al. Magnetic resonance fingerprinting. *Nature* 2013;495:187–192.
103. Chen Y, Jiang Y, Pahwa S, et al. MR fingerprinting for rapid quantitative abdominal imaging. *Radiology* 2016;279:278–286
104. Yu AC, Badve C, Ponsky LE, et al. Development of a combined MR fingerprinting and diffusion examination for prostate cancer. *Radiology* 2017;283:729–738
105. Badve C, Yu A, Dastmalchian S, et al. MR fingerprinting of adult brain tumors: Initial experience. *Am J Neuroradiol* 2017;38:492–499
106. Keenan KE, Ainslie M, Barker AJ, et al. Quantitative magnetic resonance imaging phantoms: A review and the need for a system phantom. *Magn Reson Med* 2017;61:48–61.
107. Davnall F, Yip CS, Ljungqvist G, et al. Assessment of tumor heterogeneity: an emerging imaging tool for clinical practice? *Insights Imaging* 2012;3:573–589.
108. Woodard GA, Ray KM, Joe BN, Price ER. Qualitative radiogenomics: association between oncotype DX test recurrence score and BI-RADS mammographic and breast MR imaging features. *Radiology* 2018;286:60–70.
109. Grimm LJ. Breast MRI radiogenomics: Current status and research implications. *J Magn Reson Imaging* 2016;43:1269–1278.
110. Mehta S, Hughes NP, Li S, et al. Radiogenomics monitoring in breast cancer identifies metabolism and immune checkpoints as early actionable mechanisms of resistance to anti-angiogenic treatment. *EBioMedicine* 2016;10:109–116.
111. Shinagare AB, Vikram R, Jaffe C, et al. Radiogenomics of clear cell renal cell carcinoma: preliminary findings of The Cancer Genome Atlas-Renal Cell Carcinoma (TCGA-RCC) Imaging Research Group. *Abdom Imaging* 2015;40:1684–1692.
112. Kickingeder P, Bonekamp D, Nowosielski M, et al. Radiogenomics of glioblastoma: machine learning-based classification of molecular characteristics by using multiparametric and multiregional MR imaging features. *Radiology* 2016;281:907–918.
113. Hu LS, Ning S, Eschbacher JM, et al. Radiogenomics to characterize regional genetic heterogeneity in glioblastoma. *Neuro Oncol* 2017;19:128–137.
114. Gourtsoyianni S, Doumou G, Prezzi D, et al. Primary rectal cancer: repeatability of global and local-regional MR imaging texture features. *Radiology* 2017:161375.